Sains Malaysiana 48(7)(2019): 1447–1457
http://dx.doi.org/10.17576/jsm-2019-4807-14

Chemical Surface Analysis on Post-Thermal Treatment of the K-OMS-2 Catalysts and Catalytic Oxidation Efficiency at Low Temperature

(Analisis Permukaan Kimia Rawatan Pasca Haba pada Mangkin K-OMS-2 dan Kecekapan Pemangkinan Pengoksidaan pada Suhu Rendah)

CHATKAMOL KAEWBUDDEE, PINIT KIDKHUNTHOD, NARONG CHANLEK, RATTABAL KHUNPHONOI & KITIROTE WANTALA*

ABSTRACT

The effect of calcination temperature on the physical and chemical properties of cryptomelane (K-OMS-2) was investigated. The K-OMS-2 was synthesized via a hydrothermal method and calcined at 200-600ºC. The catalytic activities of the K-OMS-2 samples were tested in packed bed reactor (PBR) on toluene oxidation. The physical and chemical properties were characterized by X-ray diffractometer (XRD), scanning electron microscopy (SEM), specific surface area computed by Brunauer-Emmett-Teller (BET) equation, Fourier-transform infrared spectroscopy (FTIR), X-ray photoelectron spectroscopy (XPS) and X-ray absorption near edge structure (XANES) techniques. The increasing of the calcination temperature from 200-600ºC led to transform the phases from MnO_2 to Mn_2O_3. The morphology of K-OMS-2 which observed in a nest-like type could promote the catalytic activity. With increasing the calcination temperature, the amount of O_{ads}/O_{latt} molar ratio slightly increased whereas OH vibrations analyzed by FTIR insignificantly increased. The comparison of interaction effect indicated that the O_{ads}/O_{latt} molar ratio played an important role in the oxidation performance more than the Mn^{3+}/Mn^{4+} molar ratio.

Keywords: Oxidation state; thermal catalysis; toluene oxidation; VOCs removal; XPS

ABSTRAK

Kesan suhu pengkalsinan pada sifat fizikal dan kimia (K-OMS-2) kriptomelan telah dikaji. K-OMS-2 telah disintesis melalui kaedah hidroterma dan dikalsin pada suhu 200-600ºC. Aktiviti sampel pemangkin K-OMS-2 diuji dalam reaktor lapisan terpadat (PBR) pada pengoksidaan toluena. Sifat fizikal dan kimia telah dicirikan oleh teknik sinar-x difraktometer (XRD), mikroskop elektron imbasan (SEM), kawasan permukaan tertentu yang dihitung melalui persamaan Brunauer-Emmett-Teller (BET), spektroskopi transformasi Fourier inframerah (FTIR), spektroskopi fotoelektron sinar-x (XPS) dan ujian penyerapan sinar- x berhampiran pinggir struktur (XANES). Peningkatan suhu pengkalsinan daripada 200-600ºC membawa kepada perubahan daripada MnO_2 kepada Mn_2O_3. Morfologi K-OMS-2 yang diperhatikan seperti jenis sarang dapat menggalakkan aktiviti pemangkinan. Dengan pertambahan suhu pengkalsinan, jumlah nisbah molar O_{ads}/O_{latt} sedikit meningkat manakala getaran OH dianalisis FTIR meningkat secara tidak bererti. Perbandingan kesan interaksi menunjukkan bahawa nisbah molar O_{ads}/O_{latt} memainkan peranan penting dalam prestasi pengoksidaan lebih daripada nisbah molar Mn^{3+}/Mn^{4+}.

Kata kunci: Keadaan pengoksidaan; pemangkin termal; pengoksidaan toluena; penyingkiran VOC; XPS

INTRODUCTION

Cryptomelane (K-OMS-2) is one of a type of octahedral molecular sieves (OMS), which is mixed-valent manganese oxides. K-OMS-2 framework structure consists of double-wide slabs of the edge-shared MnO_4^{8-} octahedral unit to form 0.46×0.46 nm tunnels with a square cross-section. The tunnels are bounded by four $Mn_2O_6^{4-}$ slabs and joined through corner-shared with each rotated 90º to its neighbor and K^+ situated in tunnel position. The mixed-valent α-MnO_2 in which charge imbalance on the octahedral framework due to the reduction of Mn^{4+} to Mn^{3+} is replaced by K^+ in the tunnel site, called the redox exchange (Feng et al. 1999). The physical and chemical properties of K-OMS-2 are porosity, various oxidation state, hydrophobic catalyst, ability to transfer oxygen, high surface area and active lattice oxygen (Brock et al. 1998; Calvert et al. 2008; Feng et al. 1999; Schurz et al. 2009; Suib 2008). Moreover, the K-OMS-2 has been widely used as a catalyst for the partial and total oxidation reactions (Chen et al. 2009; De Luna et al. 2017; Hou et al. 2013a; Mahdavi & Soleimani 2014; Millanar et al. 2018). The K-OMS-2 is an active catalyst for complete oxidation reaction at high reaction temperatures, for examples 100% selectivity to CO_2 at 400ºC for oxidation of ethyl acetate (Gandhe et al. 2007), 100% conversion of benzene (Luo et al. 2000), toluene (Liu et al. 2017; Santos et al. 2010), ethyl acetate (Liu et al. 2017), ethanol (Wang & Li 2010) and CO (Fu et al. 2017) at 300, >350, >250, 220 and 150ºC, respectively. Since

the mixed oxidation states of manganese oxide including Mn^{2+}, Mn^{3+}, Mn^{4+} and adsorbed oxygen are influencing parameters on VOCs oxidation (Hou et al. 2013a; Jia et al. 2016; Wang et al. 2015), it was found that at a high Mn^{3+}/Mn^{4+} atomic ratio of OMS-2, it can enhance the catalytic activity of benzene (Hou et al. 2013b). Additionally, the surface adsorbed oxygen (O_{ads}) and lattice oxygen (O_{latt}) are influencing on the catalytic activity. The increasing of O_{ads}/O_{latt} molar ratio of OMS-2 samples leads to increase the combustion activities of DME and toluene (Sun et al. 2017). In addition, the surface area also affects the catalytic activity on benzene oxidation (Hou et al. 2014).

K-OMS-2 can be synthesized by several methods such as reflux, solid-state chemical reactions, sol-gel and hydrothermal treatment (Ghosh et al. 2006; King'ondu et al. 2011; Said et al. 2014; Soares et al. 2018; Sun et al. 2011; Wang & Li 2009; Yu et al. 2008). The different synthesis methods affect the physical and chemical properties of K-OMS-2 (Ghosh et al. 2006). Additionally, the preparation methods play an essential role in catalytic performance (Soares et al. 2018). Among them, K-OMS-2 which synthesized by the hydrothermal method shows high Mn^{3+}/Mn^{4+} and O_{ads}/O_{latt} molar ratios to give the high efficiency of the chlorotoluene oxidation (Deng et al. 2014). Shanthakumar et al. (2009), demonstrated that OMS-2 prepared by the hydrothermal method exhibits higher styrene conversion comparing with OMS-2 synthesized by solvent-free, sol-gel and reflux methods, and give a 100% selectivity for the ring opening.

The influence of calcination temperature on the physical and chemical properties of K-OMS-2 is investigated. Conventional and reflux methods for preparation of K-OMS-2 is necessary to calcine at high temperature for its stability and activated phase (Li et al. 2011). El-Sawy et al. (2014) reported that time and temperature play an important role in nucleation and growth of crystalline OMS-2 phase. The pure OMS-2 is obtained at the calcination temperature in the range of 500-750ºC (El-Sawy et al. 2014). Additionally, the preparation of active K-OMS-2 should be calcined at 600ºC for the partial aerobic oxidation of benzyl alcohol (Schurz et al. 2009). The phase transformation of manganese oxide calcined in the air with increasing calcination temperatures is following: MnO_2, Mn_2O_3, Mn_3O_4 and MnO. At higher calcination temperature, the oxidation state of manganese is reduced from Mn^{4+} to Mn^{3+}, and eventually, Mn^{2+} (Stobbe et al. 1999). Thus, the calcination temperature is a crucial factor for the physicochemical properties and its performance.

Recently, our previous work found a novel uncalcined route for active K-OMS-2. The synthesis was carried out through the hydrothermal method without calcination process. The optimum aging temperature and time for the active K-OMS-2 sample showed a high surface area and Mn^{3+}/Mn^{4+} molar ratio, resulting in high catalytic activity. However, the uncalcined K-OMS-2 catalyst took a high reaction temperature at 250°C to complete benzene oxidation (Yodsa-nga et al. 2015). However, the pure phase of K-OMS-2 and high Mn^{3+}/Mn^{4+} molar ratio of K-OMS-2 catalyst, affecting to the catalytic activity, are depended on the calcination temperature. Consequently, this research aimed to study the effect of calcination temperature on the physical and chemical properties of K-OMS-2 and its performance. The catalytic activities were evaluated on toluene oxidation reaction in packed bed reactor (PBR). Moreover, the effect of calcination temperature on the specific surface area, Mn^{3+}/Mn^{4+} molar ratio and O_{ads}/O_{latt} molar ratio was discussed on catalytic oxidation performances. The characterizations were measured by X-ray diffractometer (XRD), scanning electron microscopy (SEM), Brunauer-Emmett-Teller (BET), Fourier transform infrared spectroscopy (FTIR), X-ray photoelectron spectroscopy (XPS) and X-ray absorption near edge structure (XANES) techniques to explain the effect of calcination temperature.

Materials and Methods

Chemicals

All the chemicals used in this study are analytical grade. Manganese acetate tetrahydrate ($Mn(CH_3COO)_2{\cdot}4H_2O$) with greater than 99% purity, potassium permanganate ($KMnO_4$) with 99% purity and glacial acetic acid (CH_3COOH) were purchased from ACROS Organics, UNIVAR and QRëC, respectively.

Cryptomelane synthesis and characterizations

Cryptomelane was synthesized by hydrothermal method following the previous work (Yodsa-nga et al. 2015). The mole ratio of $KMnO_4/Mn(CH_3COO)_2$ was fixed at 0.75. Firstly, the $KMnO_4$ solution was added to $Mn(CH_3COO)_2$ solution under continuous stirring. The pH of the mixed solution was adjusted by using acetic acid glacial to obtain an acidic condition (pH<3.5) and then transferred into an autoclave for the hydrothermal process at 75ºC for 21 h. The obtained black slurry was then filtrated and washed with deionized water until the filtrate was pH neutral. The obtained precipitate was dried at 100ºC for 4 h and then calcined at different temperatures (200-600ºC). The obtained catalysts were labeled as K-OMS-2_XXXºC, where XXXºC represents calcination temperature. The crystalline phase of the samples was analyzed by X-ray diffractometer (XRD), PANalytical, EMPYREAN, Netherlands using Cu Kα (λ = 0.1514 nm) as the X-ray source, operated at 40 mA and 45 kV. The surface morphology was characterized by scanning electron microscopy (SEM, HITACHI S-3400N, Japan). The specific surface area was analyzed by N_2 adsorption-desorption analyzer (ASAP2460, Micromeritics, USA) and calculated by Brunauer-Emmett-Teller (BET) model. The vibrations of chemical property were identified by using Fourier transform infrared spectroscopy (FTIR, TENSOR27, Bruker with ATR mode, Germany). The oxidation states of manganese and oxygen were determined by X-ray photoelectron spectroscopy (XPS) and X-ray absorption near edge structure (XANES) techniques (BL5.3

and SUT-NANOTEC-SLRI: BL5.2, respectively), Synchrotron Light Research Institute (Public Organization), Thailand.

TOLUENE DEGRADATION

The catalytic activities of K-OMS-2 samples were tested in toluene degradation via packed bed reactor (PBR) as shown in Figure 1. About 0.01 g of catalysts were placed in the center of the PBR. Toluene was maintained at -3ºC, using the cold bath as an evaporator. Approximately 7,550 ppmV of toluene concentration, calculated following Doucet et al. (2006), was studied. The hysteresis loop of reaction temperature was investigated with an increase and decrease in the range of 130-350ºC and the weight hourly space velocity (WHSV) was used at 3.41 h^{-1}. Remained concentration of toluene in the fluid was measured by gas chromatography technique with thermal conductivity detector using Gaskuropack 54 as a column (GC-TCD, Shimadzu, 8A series, Japan) which repeatedly tested at least 3 times for each experiment. The percent removal of toluene was calculated by (1).

$$\text{Percent removal of toluene} = \frac{C_0 - C_f}{C_0} \times 100 \qquad (1)$$

where C_0 and C_f are initial and final toluene concentrations, respectively.

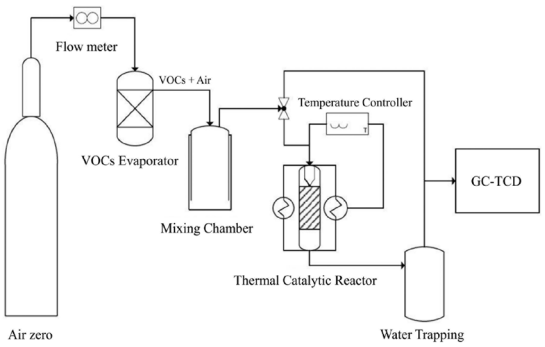

FIGURE 1. Set-up of toluene thermal-catalytic oxidation

RESULTS AND DISCUSSION

The crystallinity was characterized by X-ray diffractometer as shown in Figure 2. All synthesized samples showed characteristic peaks at 2θ values of 12.7, 18.1, 28.7, 37.5, 41.8 and 50.0º, corresponding to the K-OMS-2 standard (JCPDS 29-1020, KMn_8O_{16}) (De Luna et al. 2017; Iyer et al. 2010; Kumar et al. 2009; Millanar et al. 2018; Yodsa-nga et al. 2015). With increasing of calcination temperature, the amount of Mn^{3+} increased representing as bixbyite phase, confirmed by 2θ peak at 55.16º and become high crystallinity of bixbyite phase at the highest calcination temperature (600ºC), which presented the XRD pattern at 23.14 and 32.94º (Chen et al. 2002). Increasing of calcination temperature from 200-600ºC induced to transform MnO_2 phase to Mn_2O_3 phase or reduce Mn^{4+} to Mn^{3+}. According to the previous studies, the reduction process step of manganese oxide phase in the air with an increase in calcination temperature can occur as follows: MnO_2, Mn_2O_3, Mn_3O_4 and MnO, respectively (Christel et al. 1997; Shi et al. 2012; Stobbe et al. 1999). The MnO_2 was first reduced to Mn_2O_3. Then, Mn_2O_3 was changed to Mn_3O_4, and afterward, Mn_3O_4 was further reduced to MnO. This phenomenon suggested that the calcination temperature influenced the manganese oxide phase in K-OMS-2.

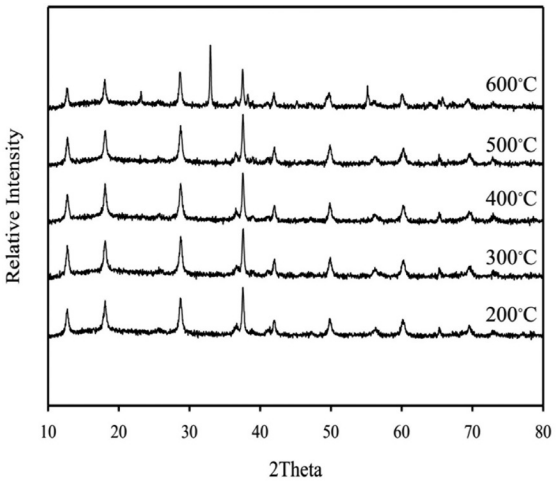

FIGURE 2. The XRD pattern of K-OMS-2 with various calcination temperatures

The calcined temperature not only affected K-OMS-2 phase but also influenced the specific surface area as shown in Table 1. The specific surface area showed an insignificant effect for the calcined samples at 200, 300, 400 and 500ºC. On the other hand, K-OMS-2_600ºC exhibited the lowest specific surface area. This result can be suggested that the high calcination temperature affected the transformation of K-OMS-2 phase to bixbyite phase, resulting in the decreasing of the specific surface area. Corresponding to Yang results, they found that the bixbyite phase of Pd/K-OMS-2 catalyst was observed when the calcined temperature was about 550ºC, and become high bixbyite crystals when the calcined temperature increased to 700ºC (Yang et al. 2010). Table 1 shows the crystallite size values that calculated by using the Scherrer equation with the reflection peaks (2θ) at 37 and 32.94º for K-OMS-2 and bixbyite samples, respectively. It can be observed that the increasing of calcination temperature over 500ºC results to decrease the specific surface area because of the annealing of K-OMS-2 and formation of bixbyite crystalline structure.

The morphologies of the samples were analyzed by SEM technique as presented in Figure 3. As can be seen, the morphology of all K-OMS-2 samples depicted the nest-like type, which are a complex arrangement of nanoscale fiber that could promote high catalytic activity.

TABLE 1. The characteristic properties of samples calcined at different temperature

Catalysts	Specific surface area (m^2/g)	$d_{crystallite}$ * (nm)	Mn^{3+}/Mn^{4+} ** molar ratio	O_{ads}/O_{latt} molar ratio
K-OMS 2_200ºC	50.88	30.63	2.45	0.28
K-OMS 2_300ºC	54.48	36.05	2.91	0.23
K-OMS 2_400ºC	49.75	40.55	3.11	0.40
K-OMS 2_500ºC	52.77	40.55	3.30	0.63
K-OMS 2_600ºC	33.00	45.76	3.65	0.46

*$d_{crystallite}$ is the crystallite site of K-OMS-2 materials which calculated by using the Scherrer equation
**Mn^{3+}/Mn^{4+} and O_{ads}/O_{latt} molar ratio were calculated by using the XPS data

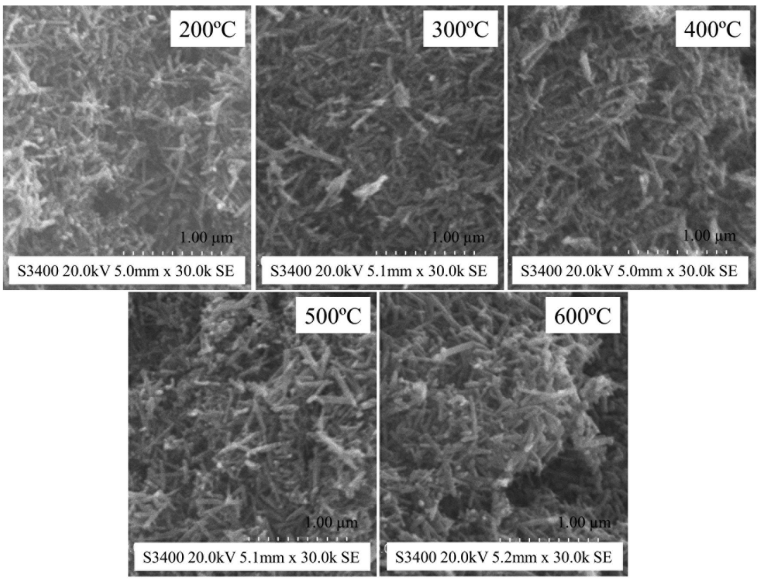

FIGURE 3. The morphology of K-OMS-2 via SEM technique

It can be confirmed that the calcination temperature between 200-600ºC showed insignificant effect on K-OMS-2 morphology. Obviously, the nanowire sizes increased with increasing calcination temperature higher than 500°C. Deng et al. (2014) found that the nest-like morphology (3.92) shows the highest Mn^{3+}/Mn^{4+} molar ratio, compared with fibrous-like (3.66) and rod-like (2.41) morphologies. Moreover, the authors also reported that the nest-like morphology (0.96) demonstrates the highest O_{ads}/O_{latt} molar ratio, while the rod-like morphology (0.73) shows the lowest amount of O_{ads}/O_{latt} molar ratio (Deng et al. 2014). Furthermore, the H_2-TPR profile displays that the TPR peak of the nest-like morphology shows the lowest temperature, resulting in the highest reducibility of manganese (Deng et al. 2014). Therefore, K-OMS-2 with the nest-like morphology could enhance the catalytic activity due to the presence of high Mn^{3+}/Mn^{4+} and O_{ads}/O_{latt} molar ratios, resulting in the high availability of active oxygen species and good mobility of oxygen species (Deng et al. 2014; Millanar et al. 2018; Yodsa-nga et al. 2015).

The catalytic activity and high-temperature stability of catalysts were investigated in packed bed reactor. Figure 4 shows the toluene removal as a function of reaction temperature hysteresis loop between 130-350ºC over various catalysts. For all K-OMS-2 samples, the heating and cooling line nearly coincided. The result showed that there was no hysteresis loop of K-OMS-2 samples. Thus, this result can be explained that the deactivation by coke formation did not occur on the catalyst surface during the reaction. Moreover, the catalyst still retained its active site (Zhang et al. 2015). The percent removal of toluene increased with increasing of reaction temperature. Additionally, the complete oxidation took place at 200ºC of the reaction temperature for the calcined samples at 200-500ºC. However, the catalytic performances of K-OMS-2 were insignificantly different, in which K-OMS-2 calcined samples at 200-400ºC, coinciding with the specific surface area values. As shown in Table 1, the specific surface area of calcined K-OMS-2 samples at 200-400ºC are 50-54 m^2/g, which are almost the same values resulted in similar to toluene removal. According to the result, K-OMS-2_500ºC presented the highest toluene removal because it displayed high specific surface area, high O_{ads}/O_{latt} and Mn^{3+}/Mn^{4+} molar ratios (Table 1). On the other hand, K-OMS-2_600ºC gave only 80% toluene removal at 200ºC of reaction temperature, because the bixbyite phase, a large particle size (Cockayne et al.

2013), was appeared in K-OMS-2 material resulting to reveal low specific surface area influenced to low O_{ads}/O_{latt} molar ratio. Likewise, Mosa et al. (2016) found that the specific surface area of the bixbyite phase material decreased with increasing the calcination temperature to 550ºC. Moreover, the specific surface area was the lowest for these material calcined at about 650ºC. Consequently, the result could also be implied that the specific surface area can play a major role in oxidation efficiency, as corresponding to the other report (Yodsa-nga et al. 2015).

The oxidation state of manganese was confirmed by XANES technique using Mn K-edge energy, as shown in Figure 5. The Mn K-edge absorption energy (E_0) of the Mn_2O_3 and MnO_2 standard was determined at 6,548 and 6,552 eV, respectively, which similar to the absorption edge energy of Wang et al. (2015). The absorption edge energy of Mn species in K-OMS-2 samples was found in the range of 6,549-6,551 eV, which slightly shifted lower than MnO_2 standard, most probably due to the presence of Mn_2O_3. Moreover, the pre-edge and white line peaks of XANES spectra showed the oxidation state of MnO_2. The shoulder peak of all calcined K-OMS-2 samples did not appear, like the spectrum of Mn_2O_3. Accordingly, the oxidation state of K-OMS-2 samples possibly displayed both Mn^{3+} and Mn^{4+}. The spectra of K-OMS-2 samples shifted toward lower energy when the calcination temperature increased. This phenomenon can cause that Mn^{4+} possibly induced to increase of the amount of Mn^{3+} during increasing calcination temperature. The XANES spectra at high photon energy (>6,555 eV) are the adsorption edge fine structure region, which identifies the absorbing atom and accurate absorber-neighbor distances (Kowalski & DeBeer 2015). Therefore, the different features and intensities at high photon energy indicated the different structure of the K-OMS-2 samples compared with manganese oxides standards. Linear combination fitting of XANES spectra with MnO_2 and Mn_2O_3 reference materials using Athena software showed that the Mn^{3+}/Mn^{4+} atomic ratios in K-OMS-2 samples increased with increasing calcined temperature as 0.43, 0.64, 0.71, 0.96 and 1.40, respectively. Yin et al. (2015) found the Mn^{3+} and Mn^{4+} atomic percent analyzed by XANES spectra in Fe-doped on K-OMS-2 samples and found that the Mn^{3+}/Mn^{4+} atomic ratios were in the range of 0.02-0.14. As our

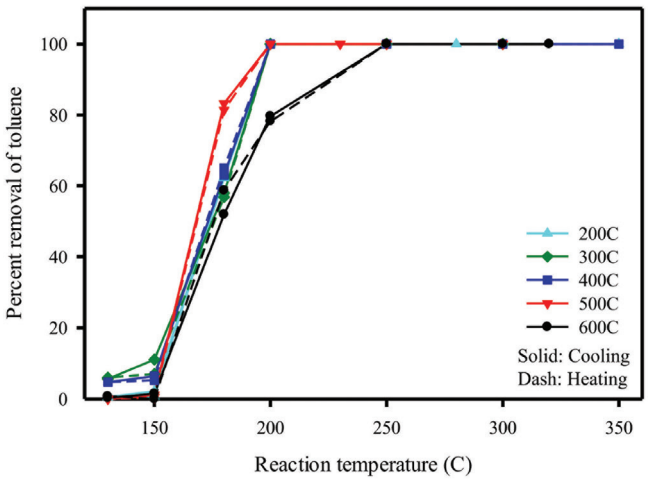

FIGURE 4. Effect of reaction temperature on the catalytic performance by toluene degradation

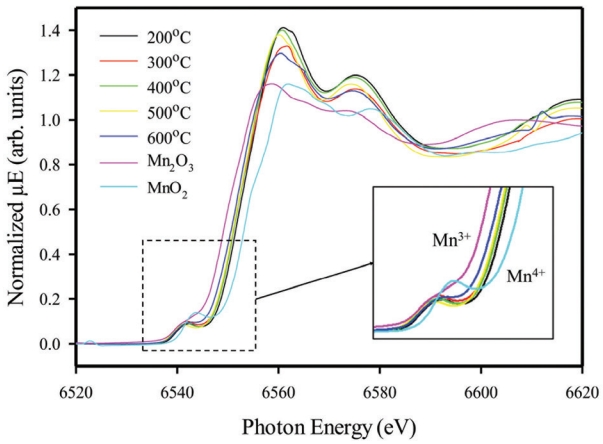

FIGURE 5. The XANES spectra of K-OMS-2 samples using K-edge energy

result, K-OMS-2_500ºC illustrated the highest reaction activity. Although K-OMS-2_600ºC showed the highest amount of Mn^{3+}/Mn^{4+} atomic ratio, it exhibited the lowest percent removal of toluene. However, the activity of K-OMS-2_600ºC on toluene oxidation completed at 250ºC, which was higher reaction temperature than other calcined temperature of K-OMS-2 catalysts. The reason for this result can explained by the presence of bixbyite phase mixed K-OMS-2 catalyst. The mixed bixbyite phase material showed not only low specific surface area but also low O_{ads}/O_{latt} molar ratio as significant parameters on performance of oxidation reaction.

Figure 6(a) displays the XPS spectra of Mn 2p and O 1s on the K-OMS-2 surface. The result revealed that Mn 2p spectra consisted of 641.96 and 643.85 eV, assigned to Mn^{3+} and Mn^{4+} species, respectively (Genuino et al. 2013; Pan et al. 2016; Sun et al. 2017, 2011; Tang et al. 2010; Yu et al. 2011). The Mn^{2+} was not found from XPS spectra, corresponded to XANES results. The Mn 2p result confirmed the co-existence of Mn^{3+} and Mn^{4+} in the K-OMS-2 samples. Additionally, the Mn^{3+}/Mn^{4+} molar ratios were calculated which based on the fitting results of the XPS spectra as shown in Table 1. With increasing calcination temperature from 200-600ºC, the amount of Mn^{3+}/Mn^{4+} molar ratio increased from 2.45-3.65. Deng et al. (2014) reported that Mn^{3+}/Mn^{4+} molar ratio is found in a range of 2.41-3.92 of K-OMS-2 synthesized by a different method. The highest Mn^{3+}/Mn^{4+} molar ratio (3.92) shows the highest efficiency of *p*-chlorotoluene oxidation. According to our result, among calcined K-OMS-2 samples, K-OMS-2_500ºC showed the highest toluene oxidation at 180ºC of reaction temperature due to the high of the Mn^{3+}/Mn^{4+} molar ratio (3.30). In addition, the existence of Mn^{3+} can associate to create the oxygen vacancies as well, which affected catalytic efficiency (Sun et al. 2017). Although, K-OMS-2_600ºC presented the highest Mn^{3+}/Mn^{4+} molar ratio (3.65) due to the main phase of bixbyite crystal, it showed low specific surface area which affected to low O_{ads}/O_{latt} molar ratio.

The O 1s spectra of the calcined K-OMS-2 samples were fitted into two peaks as displayed in Figure 6(b). The peak at lower binding energy, located at 529.57 eV was identified to the lattice oxygen. The peak at higher binding energy, located at 531.71 eV was associated with surface adsorbed oxygen, OH groups and oxygen vacancies (Dong et al. 2017; Genuino et al. 2013; Sun et al. 2017, 2011; Tang et al. 2010; Xie et al. 2016; Yu et al. 2011). Nevertheless, the adsorbed molecular water species (O_{wat}) did not appear in the calcined K-OMS-2 samples, since K-OMS-2 samples were calcined at high temperature (200-600ºC), then the adsorbed molecular water species might lose during the synthetic method. Moreover, Jia et al. (2016) reported that there are only two kinds of lattice oxygen and surface adsorbed species on the surface of the α-MnO_2 nanostructure.

Generally, the oxygen on the surface of K-OMS-2 was accorded to oxygen (O_{ads}) and water (O_{wat}) adsorptions.

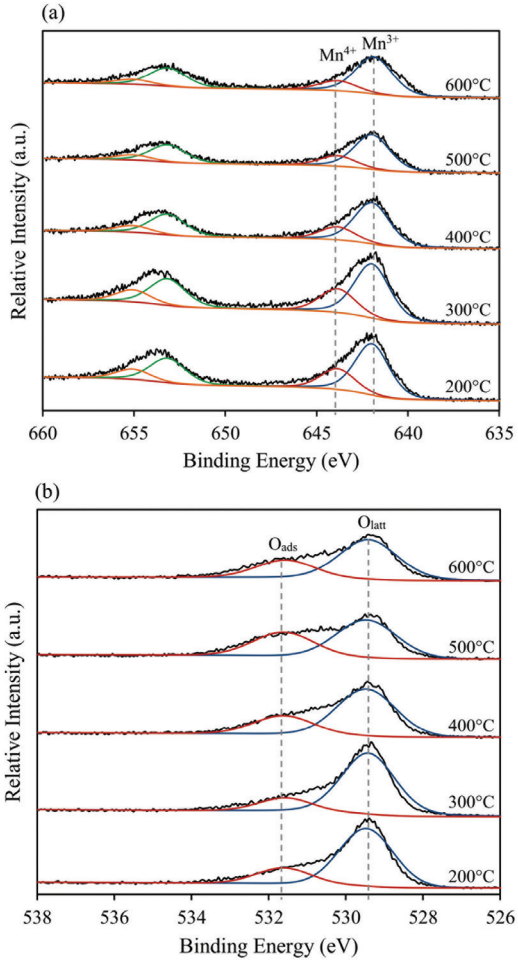

FIGURE 6. The XPS spectra of (a) Mn2p and (b) O1s of K-OMS-2 samples with various calcined temperature

Thus, the confirmation of the O_{ads} specific adsorb on the surface was examined. The OH group was measured from the lattice vibrational behavior of materials by using FTIR spectroscopy to probe its spectral features. The spectra can be separated into three groups of the lattice vibrational behaviors of the K-OMS-2 catalyst. Firstly, the signature of the K-OMS-2 structure presented the lattice vibration modes of Mn–O bond in (MnO_6) octahedral framework which appeared the characteristic bands at ~700-400 cm^{-1}. Secondly, the bending vibration of the hydroxy groups in tunnel structure represented the water molecules and OH groups that observed at ~1600 cm^{-1}. Thirdly, the broadband detected at approximately 3300 cm^{-1} was assigned to the stretching vibration of the hydroxy groups in the lattice of the K-OMS-2 structure (Ousmane et al. 2014; Said et al. 2018, 2016; Zhang et al. 2012). The FTIR spectra of calcined K-OMS-2 samples with and without drying process (105ºC for overnight) in the range of 600-4000 cm^{-1} is displayed in Figure 7(a) and 7(b), respectively. The results showed that the characteristic vibrations of calcined K-OMS-2 samples appeared at ~706 cm^{-1} which may present the lattice vibrational behavior of Mn–O lattice vibration mode in MnO_6 octahedron in K-OMS-2 material.

The calcined K-OMS-2 samples without drying process (as shown in Figure 7(b)) similarly exhibited low intensities of the vibrational behavior at 1624 cm^{-1} which specified to the adsorbed water molecules from atmospheric humidity in the tunnel structure of K-OMS-2 material. Additionally, the intensities of adsorbed water did not increase with increasing the calcination temperatures. Whereas, the adsorbed water molecules were not observed on the samples with the drying process (Figure 7(a)). Broadband at 3300 cm^{-1} of both Figure 7(a) and 7(b) was not detected owing to the absence of hydroxyl groups or adsorbed water molecules in the lattice of calcined K-OMS-2 materials agreeing with Ousmane et al. (2014) report. The peak at 1627 cm^{-1} was not found, described as no adsorbed water in the K-OMS-2 tunnels. Therefore, the result can be concluded that the adsorbed molecular water in both tunnel and lattice K-OMS-2 structures in all calcination temperatures were insignificant on O_{ads} results.

According to our results, the adsorbed molecular water did not occur in the calcined K-OMS-2 samples. Besides, the highest composition of adsorbed molecular water shows the lowest catalytic activity (Genuino et al. 2013). Therefore, we could predicate that the K-OMS-2 sample is a hydrophobic catalyst, which is a gainful catalyst for complete oxidation of VOCs to CO_2 and H_2O. As shown in Table 1, the O_{ads}/O_{latt} molar ratio was estimated from the XPS results. The O_{ads}/O_{latt} molar ratio increased (0.28-0.63) with increasing calcination temperature from 200-500ºC, and then decreased (0.46) at 600ºC of calcination temperature. Deng et al. (2014) reported that the increasing of Mn^{3+}/Mn^{4+} molar ratio resulted in increasing O_{ads}/O_{latt} molar ratio. Considering over K-OMS-2_600ºC, it was found that the sample illustrated the low specific surface area and low O_{ads}/O_{latt} molar ratio, resulting in low catalytic activity. The surface adsorbed oxygen species is regarded to be strongly electrophilic that could attract an organic molecule (Sun et al. 2015). It also showed in higher mobility than the lattice oxygen species. Therefore, the catalyst with higher surface adsorbed oxygen can give higher catalyst activity.

The contour plot of percent toluene removal as a function of Mn^{3+}/Mn^{4+} molar ratio and the specific surface area is shown in Figure 8(a). The higher Mn^{3+}/Mn^{4+} molar ratio (2.45-3.65) and higher specific surface area demonstrated the higher efficiency of toluene removal. Likewise, Figure 8(b) displays the effect of O_{ads}/O_{latt} molar ratio and specific surface area on percent toluene removal. The results showed that with increasing of O_{ads}/O_{latt} molar ratio (0.28-0.63) and specific surface area resulted in increasing percent removal of toluene. The contour plot clearly explained the relationship between Mn^{3+}/Mn^{4+} and O_{ads}/O_{latt} molar ratio as demonstrated in Figure 8(c). Besides, the results were found that in cases of high Mn^{3+}/Mn^{4+} molar ratio and low O_{ads}/O_{latt} molar ratio affected low percent removal of toluene because of the low specific surface area. On the other hand, the lower Mn^{3+}/Mn^{4+} molar ratio and higher O_{ads}/O_{latt} molar ratio presented a higher

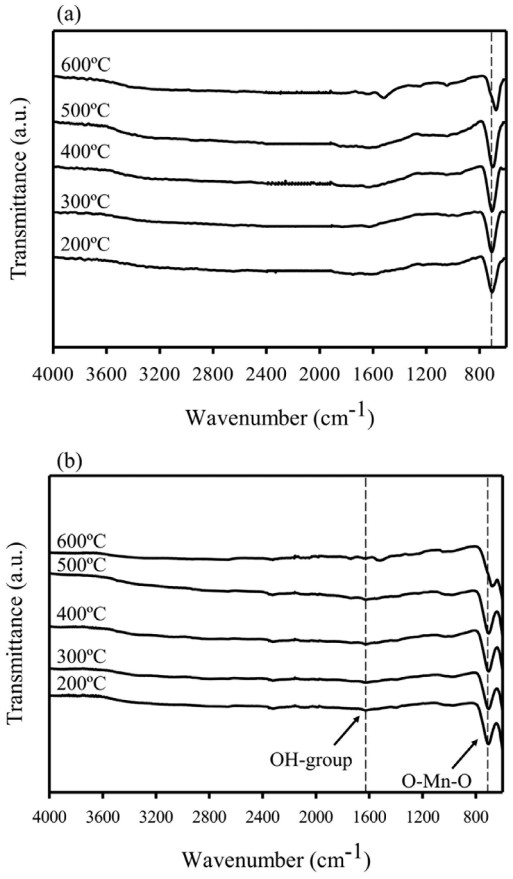

FIGURE 7. The FTIR spectra of calcined K-OMS-2 samples (a) with and (b) without drying process

performance of toluene removal. This result can cause the O_{ads}/O_{latt} molar ratio which related to the specific surface area. Therefore, the experimental results can be concluded that the specific surface area presented a significant factor on the O_{ads}/O_{latt} molar ratio and performance of K-OMS-2 (Yodsa-nga et al. 2015).

Therefore, the result can be proposed that the calcination temperature of K-OMS-2 affect the physical and chemical properties, which subsequently influenced the reactivity of toluene removal. The presence of Mn^{3+} in K-OMS-2 described that oxygen vacancies could generate to maintain electrostatic balance in structures (Fang et al. 2017). The increasing of calcination temperature (up to 500ºC) increases the amount of Mn^{3+}/Mn^{4+} molar ratio, increasing O_{ads}/O_{latt} molar ratio. Subsequently, it can enhance the toluene removal. However, it should be noted that the K-OMS-2 catalyst was changed to bixbyite phase during increasing calcination temperature to 600ºC. This observed result can cause the reduction of toluene removal by decreasing the specific surface area and O_{ads}/O_{latt} molar ratio.

CONCLUSION

The effect of calcination temperature influenced the physical and chemical properties of the K-OMS-2 catalyst.

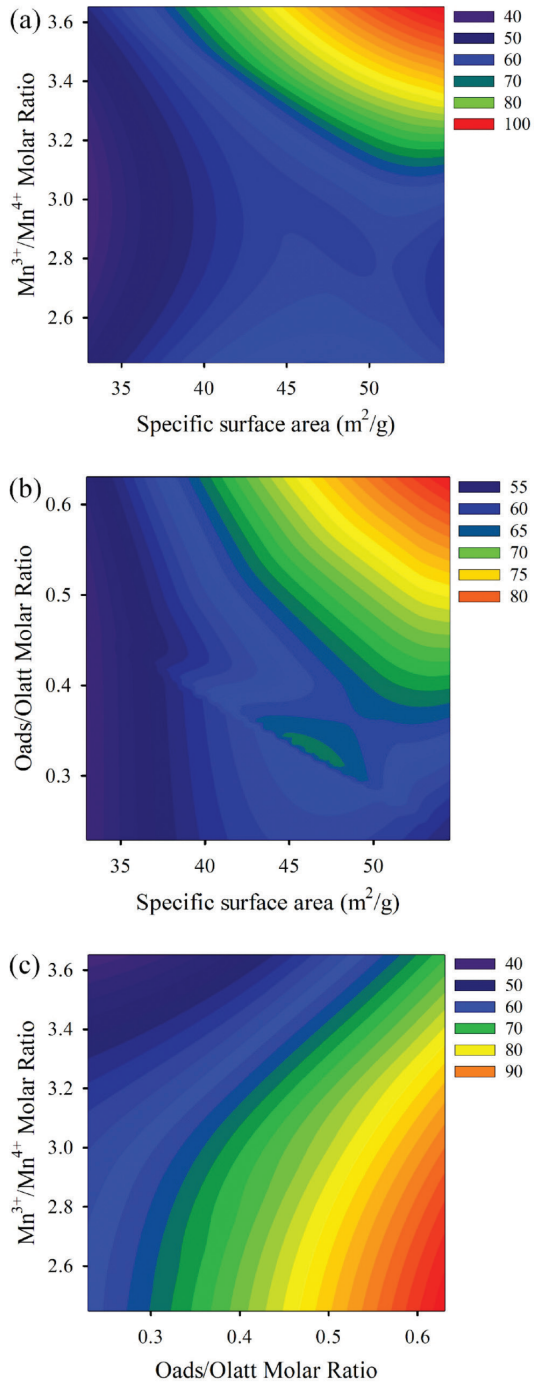

FIGURE 8. Contour plot of percent toluene removal on effect of (a) Mn^{3+}/Mn^{4+} molar ratio and specific surface area (b) O_{ads}/O_{latt} molar ratio and specific surface area (c) Mn^{3+}/Mn^{4+} molar ratio and O_{ads}/O_{latt} molar ratio (Mn^{3+}/Mn^{4+} and O_{ads}/O_{latt} molar ratio from XPS data)

At higher than 500ºC of calcination temperature, the phase transformation of K-OMS-2 to bixbyite was found. Additionally, the specific surface area and O_{ads}/O_{latt} molar ratio decreased as well, which led to the low efficiency of toluene removal. The O_{ads} referred to only adsorbed oxygens confirmed by FTIR spectra. The oxidation state of K-OMS-2 presented the Mn^{3+} and Mn^{4+} as confirmed by XANES and XPS techniques. The Mn^{3+}/Mn^{4+} and O_{ads}/O_{latt} molar ratios increased with increasing calcination temperature. On the contrary, O_{ads}/O_{latt} molar ratio decreased when the calcination temperature was 600ºC, which affected the decreasing of the catalytic activity. The toluene oxidation strongly depended on the specific surface area and the O_{ads}/O_{latt} molar ratio more than Mn^{3+}/Mn^{4+} molar ratio. The most appropriate calcination temperature of K-OMS-2 synthesis was 500ºC.

ACKNOWLEDGEMENTS

Authors would like to acknowledge the financial support from Research Center for Environmental and Hazardous Substance Management (EHSM) and Graduate School, Khon Kaen University for supporting lecturer to admit high potential student to study and research on his expert program Year 2015 (Research No. 582T266) and the Office of Higher Education Commission (OHEC) and the S&T Postgraduate Education and Research Development Office (PERDO) through Research Program on Development of Appropriate Technologies for Coloring Agent Removal from Textile Dyeing, Pulp & Paper, Sugar Industries for Sustainable Management, Center of Excellence on Hazardous Substance Management (HSM), Chulalongkorn University, Bangkok 10330, Thailand. The authors would also like to express their gratitude to Synchrotron Light Research Institute Public Organization, Thailand for XPS measurement (BL. 5.2 and BL. 5.3) and the Center of Excellence on Hazardous Substance Management (HSM) Chulalongkorn University and the Advanced Functional nanomaterials & Membrane for Environmental Remediation (AFMER) Research Unit for their invaluable support in terms of facilities and scientific equipment.

REFERENCES

Brock, S.L., Duan, N., Tian, Z.R., Giraldo, O., Hua, Z. & Suib, S.L. 1998. A review of porous manganese oxide materials. *Chemistry of Materials* 10(10): 2619-2628.

Calvert, C., Joesten, R., Ngala, K., Villegas, J., Morey, A., Shen, X. & Suib S.L. 2008. Synthesis, characterization, and rietveld refinement of tungsten-framework-doped porous manganese oxide (K-OMS-2) material. *Chemistry of Materials* 20(20): 6382-6388.

Chen, T., Dou, H., Li, X., Tang, X., Li, J. & Hao, J. 2009. Tunnel structure effect of manganese oxides in complete oxidation of formaldehyde. *Microporous and Mesoporous Materials* 122(1-3): 270-274.

Chen, X., Shen, Y.F., Suib, S.L. & O'Young, C.L. 2002 Characterization of manganese oxide octahedral molecular sieve (M-OMS-2) materials with different metal cation dopants. *Chemistry of Materials* 14(2): 940-948.

Christel, L., Pierre, A. & Abel, D.A.M.R. 1997. Temperature programmed reduction studies of nickel manganite spinels. *Thermochimica Acta* 306(1-2): 51-59.

Cockayne, E., Levin, I., Wu, H. & Llobet, A. 2013. Magnetic structure of bixbyite α-Mn2O3: A combined DET+U and neutron diffraction study. *Physical Review B* 87(18): 184413.

De Luna, M.D., Millanar, J., Yodsa-nga, A. & Wantala, K., 2017. Gas phase catalytic oxidation of VOCS using hydrothermally synthesized nest-like K-OMS 2 catalyst. *Sains Malasiana* 46(2): 275-283.

Deng, Y.Q., Zhang, T., Au, C.T. & Yin, S.F. 2014. Oxidation of p-chlorotoluene to p-chlorobenzaldehyde over manganese-based octahedral molecular sieves of different morphologies. *Catalysis Communications* 43: 126-130.

Dong, C., Liu, X., Guan, H., Xiao, X. & Wang, Y. 2017. Combustion synthesized hierarchically porous Mn_3O_4 for catalytic degradation of methyl orange. *The Canadian Journal of Chemical Engineering* 95(4): 643-647.

Doucet, N., Bocquillon, F., Zahraa, O. & Bouchy, M. 2006. Kinetics of photocatalytic VOCs abatement in a standardized reactor. *Chemosphere* 65(7): 1188-1196.

El-Sawy, A.M., King'ondu, C.K., Kuo, C.H., Kriz, D.A., Guild, C.J., Meng, Y., Frueh, S.J., Dharmarathna, S., Ehrlich, S.N. & Suib, S.L. 2014. X-ray absorption spectroscopic study of a highly thermally stable manganese oxide octahedral molecular sieve (OMS-2) with high oxygen reduction reaction activity. *Chemistry of Materials* 26(19): 5752-5760.

Fang, J., Li, J., Gao, L., Jiang, X., Zhang, J, Xu, A. & Li, X. 2017. Synthesis of OMS-2/graphite nanocomposites with enhanced activity for pollutants degradation in the presence of peroxymonosulfate. *Journal of Colloid and Interface Science* 494: 185-193.

Feng, Q., Kanoh, H. & Ooi, K. 1999. Manganese oxide porous crystals. *Journal of Materials Chemistry* 9(2): 319-333.

Fu, Z., Liu, L., Song, Y., Ye, Q., Cheng, S., Kang, T. & Dai, H. 2017. Catalytic oxidation of carbon monoxide, toluene, and ethyl acetate over the xPd/OMS-2 catalysts: Effect of Pd loading. *Frontiers of Chemical Science and Engineering* 11(2): 185-196.

Gandhe, A.R., Rebello, J.S., Figueiredo, J.L. & Fernandes, J.B. 2007. Manganese oxide OMS-2 as an effective catalyst for total oxidation of ethyl acetate. *Applied Catalysis B: Environmental* 72(1-2): 129-135.

Genuino, H.C., Meng, Y., Horvath, D.T., Kuo, C.H., Seraji, M.S., Morey, A.M., Joesten, R.L. & Suib, S.L. 2013. Enhancement of catalytic activities of octahedral molecular sieve manganese oxide for total and preferential CO oxidation through vanadium ion framework substitution. *ChemCatChem* 5(8): 2306-2317.

Ghosh, R., Shen, X., Villegas, J.C., Ding, Y., Malinger, K. & Suib, S.L. 2006. Role of manganese oxide octahedral molecular sieves in styrene epoxidation. *The Journal of Physical Chemistry B* 110(14): 7592-7599.

Hou, J., Li, Y., Mao, M., Zhao, X. & Yue, Y. 2014. The effect of Ce ion substituted OMS-2 nanostructure in catalytic activity for benzene oxidation. *Nanoscale* 6(24): 15048-15058.

Hou, J., Li, Y., Liu, L., Ren, L. & Zhao, X. 2013a. Effect of giant oxygen vacancy defects on the catalytic oxidation of OMS-2 nanorods. *Journal of Materials Chemistry A* 1(23): 6736-6741.

Hou, J., Liu, L., Li, Y., Mao, M., Lv, H. & Zhao, X. 2013b. Tuning the K^+ concentration in the tunnel of OMS-2 nanorods leads to a significant enhancement of the catalytic activity for benzene oxidation. *Environmental Science & Technology* 47(23): 13730-13736.

Iyer, A., Galindo, H., Sithambaram, S., King'ondu, C., Chen, C.H. & Suib, S.L. 2010. Nanoscale manganese oxide octahedral molecular sieves (OMS-2) as efficient photocatalysts in 2-propanol oxidation. *Applied Catalysis A: General* 375(2): 295-302.

Jia, J., Zhang, P. & Chen, L. 2016. The effect of morphology of α-MnO_2 on catalytic decomposition of gaseous ozone. *Catalysis Science & Technology* 6(15): 5841-5847.

King'ondu, C.K., Opembe, N., Chen, C.H., Ngala, K., Huang, H., Iyer, A., Garces, H.F. & Suib, S.L. 2011. Manganese oxide octahedral molecular sieves (OMS-2) multiple framework substitutions: A new route to OMS-2 particle size and morphology control. *Advanced Functional Materials* 21(2): 312-323.

Kowalski, J. & DeBeer, S. 2015 The role of X-ray spectroscopy in understanding the geometric and electronic structure of nitrogenase. *Biochimica et Biophysica Acta* 1853(6): 1406-1415.

Kumar, R., Sithambaram, S. & Suib, S.L. 2009. Cyclohexane oxidation catalyzed by manganese oxide octahedral molecular sieves - Effect of acidity of the catalyst. *Journal of Catalysis* 262(2): 304-313.

Li, D.Y., Liu, H.D. & Chen, Y.F. 2011. Synthesis of manganese oxide octahedral molecular sieve and their application in catalytic oxidation of benzene. *Huan Jing Ke Xue= Huanjing Kexue* 32(12): 3657-3661.

Liu, L., Song, Y., Fu, Z., Ye, Q., Cheng, S., Kang, T. & Dai, H. 2017. Effect of preparation method on the surface characteristics and activity of the Pd/OMS-2 catalysts for the oxidation of carbon monoxide, toluene, and ethyl acetate. *Applied Surface Science* 396: 599-608.

Luo, J., Zhang, Q., Huang, A. & Suib, S.L. 2000. Total oxidation of volatile organic compounds with hydrophobic cryptomelane-type octahedral molecular sieves. *Microporous and Mesoporous Materials* 35-36: 209-217.

Mahdavi, V. & Soleimani, S. 2014. Novel synthesis of manganese and vanadium mixed oxide (V_2O_5/OMS-2) as an efficient and selective catalyst for the oxidation of alcohols in liquid phase. *Materials Research Bulletin* 51: 153-160.

Millanar, J.M., De Luna, M.D.G., Yodsa-Nga, A. & Wantala, K. 2018. Toluene oxidation using K-OMS-2 synthesized via hydrothermal process by central composite design. *Chiang Mai Journal of Science* 45(2): 1030-1038.

Mosa, I.M., Biswas, S., El-Sawy, A.M., Botu, V., Guild, C., Song, W., Ramprasad, R., Rusling, J. & Suib, S.L. 2015. Tunable mesoporous manganese oxide for high performance oxygen reduction and evolution reactions. *Journal of Materials Chemistry A* 4(2): 620-631.

Ousmane, M., Perrussel, G., Yan, Z., Clacens, J.M., De Campo, F. & Pera-Titus, M. 2014. Highly selective direct amination of primary alcohols over a Pd/K-OMS-2 catalyst. *Journal of Catalysis* 309: 439-452.

Pan, F., Liu, W., Yu, Y., Yin, X., Wang, Q., Zheng, Z., Wu, M., Zhao, D., Zhang, Q., Lei, X. & Xia, D. 2016. The effects of manganese oxide octahedral molecular sieve chitosan microspheres on sludge bacterial community structures during sewage biological treatment. *Scientific Reports* 6(1): 37518.

Said, S., Maghrabi, H.H.E., Riad, M. & Mikhail, S. 2018. Photo-catalytic selective organic transformations by Fe-doped octahedral molecular sieves (manganese oxide) nano-structure. *Journal of Asian Ceramic Societies* 6(2): 169-181.

Said, S., Riad, M., Helmy, M., Mikhail, S. & Khalil, L. 2016. Preparation of nano-structured cryptomelane materials for catalytic oxidation reactions. *Journal of Nanostructure in Chemistry* 6(2): 171-182.

Said, S., Riad, M., Helmy, M., Mikhail, S. & Khalil, L. 2014. Effect of the different preparation methods on the characterization

and the catalytic activity of the nano-structured cryptomelane materials. *Chemistry and Materials Research* 6(12): 27-41.

Santos, V.P., Bastos, S.S.T., Pereira, M.F.R., Orfao, J.J.M. & Figueiredo, J.L. 2010. Stability of a cryptomelane catalyst in the oxidation of toluene. *Catalysis Today* 154(3-4): 308-311.

Schurz, F., Bauchert, J.M., Merker, T., Schleid, T., Hasse, H. & Glaser, R. 2009. Octahedral molecular sieves of the type K-OMS-2 with different particle sizes and morphologies: Impact on the catalytic properties in the aerobic partial oxidation of benzyl alcohol. *Applied Catalysis A: General* 355(1-2): 42-49.

Shi, F., Wang, F., Dai, H., Dai, J., Deng, J., Liu, Y., Bai, G., Ji, K. & Au, C.T. 2012. Rod-, flower-, and dumbbell-like MnO2: Highly active catalysts for the combustion of toluene. *Applied Catalysis A: General* 433-434: 206-213.

Shanthakumar, S., Xu, L., Chen, C.H., Ding, Y., Kumar, R., Calvert, C. & Suib, S.L. 2009. Manganese octahedral molecular sieve catalysts for selective styrene oxide ring opening. *Catalysis Today* 140(3-4): 162-168.

Soares, O.S.G.P., Rocha, R.P., Orfao, J.J.M., Pereira, M.F.R. & Figueiredo, J.L. 2018. Ethyl and butyl acetate oxidation over manganese oxides. *Chinese Journal of Catalysis* 39(1): 27-36.

Stobbe, E.R., de Boer, B.A. & Geus, J.W. 1999. The reduction and oxidation behaviour of manganese oxides. *Catalysis Today* 47(1-4): 161-167.

Suib, S.L. 2008. Structure, porosity, and redox in porous manganese oxide octahedral layer and molecular sieve materials. *Journal of Materials Chemistry* 18(14): 1623-1631.

Sun, H., Liu, Z., Chen, S. & Quan, X. 2015. The role of lattice oxygen on the activity and selectivity of the OMS-2 catalyst for the total oxidation of toluene. *Chemical Engineering Journal* 270: 58-65.

Sun, H., Chen, S., Wang, P. & Quan, X. 2011. Catalytic oxidation of toluene over manganese oxide octahedral molecular sieves (OMS-2) synthesized by different methods. *Chemical Engineering Journal* 178: 191-196.

Sun, L., Cao, Q., Hu, B., Li, J., Hao, J., Jing, G. & Tang, X. 2011. Synthesis, characterization and catalytic activities of vanadium-cryptomelane manganese oxides in low-temperature NO reduction with NH3. *Applied Catalysis A: General* 393(1-2): 323-330.

Sun, M., Zhang, B., Liu, H., He, B., Ye, F., Yu, L., Sun, C. & Wen, H. 2017. The effect of acid/alkali treatment on the catalytic combustion activity of manganese oxide octahedral molecular sieves. *RSC Advances* 7(7): 3958-3965.

Tang, X., Li, J. & Hao, J. 2010. Significant enhancement of catalytic activities of manganese oxide octahedral molecular sieve by marginal amount of doping vanadium. *Catalysis Communications* 11(10): 871-875.

Wang, C., Ma, J., Liu, F., He, H. & Zhang, R. 2015. The effects of Mn2+ precursors on the structure and ozone decomposition activity of cryptomelane-type manganese oxide (OMS-2) catalysts. *The Journal of Physical Chemistry C* 119(40): 23119-23126.

Wang, R. & Li, J. 2010. Effects of precursor and sulfation on OMS-2 catalyst for oxidation of ethanol and acetaldehyde at low temperatures. *Environmental Science & Technology* 44(11): 4282-4287.

Wang, R. & Li, J. 2009. OMS-2 catalysts for formaldehyde oxidation: Effects of Ce and Pt on structure and performance of the catalysts. *Catalysis Letters* 131(3-4): 500-505.

Xie, Y., Guo, Y., Guo, Y., Wang, L., Zhan, W., Wang, Y., Gong, X. & Lu, G. 2016. A highly effective Ni-modified MnOx catalyst for total oxidation of propane: The promotional role of nickel oxide. *RSC Advances* 6(55): 50228-50237.

Yang, X., Han, J., Du, Z., Yuan, H., Jin, F. & Wu, Y. 2010. Effect of Pb dopant on structure and activity of Pd/K-OMS-2 catalysts for heterogeneous oxidative carbonylation of phenol. *Catalysis Communications* 11(7): 643-646.

Yin, H., Dai, X., Zhu, M., Li, F., Feng, X. & Liu, F. 2015. Fe-doped cryptomelane synthesized by refluxing at atmosphere: Structure, properties and photocatalytic degradation of phenol. *Journal of Hazardous Materials* 296: 221-229.

Yodsa-nga, A., Millanar, J.M., Neramittagapong, A., Khemthong, P. & Wantala, K. 2015. Effect of manganese oxidative species in as-synthesized K-OMS-2 on the oxidation of benzene. *Surface and Coatings Technology* 271: 217-224.

Yu, L., Diao, G., Ye, F., Sun, M., Zhou, J., Li, Y. & Liu, Y. 2011. Promoting effect of Ce in Ce/OMS-2 catalyst for catalytic combustion of dimethyl ether. *Catalysis Letters* 141(1): 111-119.

Yu, L., Sun, M., Yu, J., Yu, Q., Hao, Z. & Li, C. 2008. Synthesis and characterization of manganese oxide octahedral molecular sieve and its catalytic performance for DME combustion. *Chinese Journal of Catalysis* 29(11): 1127-1132.

Zhang, Q., Wang, M., Zhang, T., Wang, Y., Tang, X. & Ning, P. 2015. A stable Ni/SBA-15 catalyst prepared by the ammonia evaporation method for dry reforming of methane. *RSC Advances* 5(114): 94016-94024.

Zhang, T., Liu, J. & Sun, D.D. 2012. A novel strategy to fabricate inorganic nanofibrous membranes for water treatment: Use of functionalized graphene oxide as a cross linker. *RSC Advances* 2(12): 5134-5137.

Chatkamol Kaewbuddee & Kitirote Wantala*
Department of Chemical Engineering
Faculty of Engineering
Khon Kaen University, Khon Kaen 40002
Thailand

Chatkamol Kaewbuddee, Rattabal Khunphonoi &
Kitirote Wantala*
Chemical Kinetics and Applied Catalysis Laboratory (CKCL)
Faculty of Engineering
Khon Kaen University, Khon Kaen 40002
Thailand

Pinit Kidkhunthod & Narong Chanlek
Synchrotron Light Research Institute Public Organization
111 University Avenue
Muang District, Nakhon Ratchasima, 30000
Thailand

Rattabal Khunphonoi
Department of Environmental Engineering
Faculty of Engineering
Khon Kaen University, Khon Kaen 40002
Thailand

Rattabal Khunphonoi & Kitirote Wantala*
Research Center for Environmental and Hazardous Substance Management (EHSM)
Faculty of Engineering
Khon Kaen University, Khon Kaen 40002
Thailand

Kitirote Wantala*
Research Program on Development of Appropriate Technologies for Coloring Agent Removal from Textile Dyeing, Pulp & Paper, Sugar Industries for Sustainable Management
Center of Excellence on Hazardous Substance Management (HSM)
Chulalongkorn University, Bangkok 10330
Thailand

*Corresponding author; email: kitirote@kku.ac.th

Received: 18 December 2018
Accepted: 24 April 2019